A Local criterion for distinguishing detonation and deflagration for pressure gain combustion

By H. A. Elasrag, J. Hoke†, B. Rankin AND S. A. Schumaker‡

Detonation and deflagration waves are compared and distinguished for hydrogen/air mixtures. Chemical explosive mode analysis (CEMA) showed that detonation is characterized by higher chemical explosive mode eigenvalues and undergoes radical explosion after the shock wave. CEMA showed that the H radical makes the largest contribution to the chemical explosive mode and can be used as an ignition indicator. A characteristic Damköhler number ($Da_{c,H}$) is then defined as the ratio of the H radical peak chemical production to peak diffusion rates. The deflagration mode consistently shows a $Da_{c,H}$ of O(1) at a wide range of operating conditions, while detonation shows a higher contribution of chemistry relative to diffusion that increases with pressure [i.e. O(100) for P = 1 bar and O(1000) for P = 10 bar]. This behavior is due to the different ignition and flame propagation mechanisms for detonation compared to deflagration. The criterion is applied successfully to one-dimensional detonation and deflagration propagating flames and to the non-premixed Air Force Research Laboratory (AFRL)'s 6-inch Rotating detonation engine over a wide range of pressures and equivalence ratios.

1. Introduction

Pressure-gain combustion (PGC) systems have many potential benefits, such as higher thermodynamic efficiency, higher specific power output and higher thrust-to-weight ratio (Wolanski 2013). The benefits are due to the rapid release of energy leading to designs that are more compact and efficient (Lu & Braun 2014). The rotating detonation engine (RDE) is a PGC design in whiche the pressure gain is achieved by a circumferentially rotating detonation wave in an annular channel (Wolanski 2013). One of the challenges, however, to achieving the required pressure gain is to minimize the non-ideal losses in the systems that reduce the total pressure gain and the overall efficiency.

Examples of non-ideal losses are pressure losses across the injectors, incomplete mixing between reactants (Rankin *et al.* 2017; Chacon & Gamba 2019) or heat release by deflagration combustion rather than by detonation combustion. Deflagration combustion involves freely propagating flames traveling at subsonic speed at almost constant pressure, while in detonation, the reactive front is coupled to, and travels at the same speed as, a leading shock wave that increases the static pressure across the flame significantly compared to the deflagration wave. In RDEs, the heat released in the deflagration mode at low pressures reduces the potential of pressure gain combustion. As such, a method to detect the heat released in each combustion mode is needed to guide design improvements. In this work, we focus on developing a low-cost efficient criterion to identify the heat release that occurs in the higher-pressure detonation mode and the heat release that occurs in the lower-pressure deflagration mode. For simplicity, we consider all reactive propagations to be either detonations or deflagrations.

† Innovative Scientific Solutions Inc.
‡ Air Force Research Laboratory, Wright-Patterson Air Force Base

Two methods are reported in the literature to distinguish the local burning combustion mode in RDEs. The first one is based on a user-defined local pressure threshold, where the heat released above the threshold is considered detonative and the heat released below the threshold is considered deflagration. Cocks *et al.* (2016) used a threshold of **5** bar, and Strakey *et al.* (2016) used a threshold value of 50% of the peak pressure. This method quantification for deflagration events, although successful, will vary with the pressure threshold used and if conditioned on different temperature ranges (Elasrag *et al.* 2022). It also ignores the possible deflagration at high pressure.

The second method is based on the chemical explosive mode analysis (CEMA) (Lu *et al.* 2010). In this method, the explosive eigenvalues are used for distinguishing between the two modes (Xu *et al.* 2019; Pal *et al.* 2020). If the local explosive eigenvalue is larger than the maximum explosive eigenvalue of a premixed freely propagating deflagration, the mode is identified as a detonation, otherwise a deflagration mode is identified. The CEMA-based method, as applied previously, uses a premixed flame at constant low pressure for calculating the distinguishing eigenvalues (Pal *et al.* 2020); therefore, deflagration that occurs in the high-pressure, post-detonation environment may not be distinguished from the detonation itself. In Section-3 we review the CEMA-based methodology and apply it to a one-dimensional, premixed and freely-propagating flame at several reactant conditions and extend the CEMA analysis to detonation based on the Zeldovich, von Neumann, and Döring (ZND) one-dimensional model (Zel'dovich 1940). The CEMA-based method was found to demarcate detonation and deflagration initiated at the same pressure.

Here, a different criterion is proposed based on a characteristic Damköhler number. Methods based on characteristic Damköhler number are common in the literature. For example, it has been used to classify deflagration from spontaneous ignition in homogeneous charge compression ignition (HCCI) and stratified charge compression ignition (SCCI) engines (Elasrag & Ju 2013; Yoo *et al.* 2013), to detect onset of stabilized oblique detonation by hypervelocity projectiles (Kaneshige & Shepherd 1996) and to detect ignition in a syngas mixture (Pal *et al.* 2020) and a lifted ethylene jet flame using CEMA (Luo *et al.* 2012). In Section-4, the characteristic Damköhler number criterion is extended to distinguish detonation and deflagration. The method is based on the observation that in deflagration mass and heat transport by diffusion controls the flame propagation, while in detonation diffusion has less effect and chemical kinetics transport is dominant (Zel'dovich 1980). A local Damköhler number is defined as the ratio of rates of production by chemical reaction to transport by diffusion. The deflagration threshold for such a Damköhler number is expected to be on the order of unity for different pressures. The criterion is verified over different inflow pressure conditions and equivalence ratios and applied to the AFRL 6-inch RDE (Rankin *et al.* 2017).

2. Detonation and deflagration wave structures

Simulations for one-dimensional nondetonative and freely propagating premixed flames for a hydrogen/air mixture are performed and compared to the one-dimensional ZND solution. The chemical source terms are calculated using a hydrogen-air reaction model with 10 species and 21 reactions (Conaire *et al.* 2004). The unburnt mixture equivalence ratio ϕ, static pressure (P) and static temperature (T) are fixed to 1.0, 1.0 bar and 300 K, respectively.

Figure 1(a) depicts the ZND wave structure (Zel'dovich 1940) solution for P =1 bar.

Similar structure can be shown for P = 10 bar. The figure shows the different ZND states across the wave structure. As the unburnt gases flow into the shock, the shock wave increases the T and P of the reactants by a ratio of 5:1 and 27:1, respectively. The distance from the shock front to the heat release peak is defined as the induction period or induction length scale Δ_i. Within Δ_i the reactants undergo chain branching reactions with very little energy released or absorbed. After the induction period, heat is released by combustion. The heat release peak is defined by the exothermic thermicity pulse length scale Δ_e with the thermicity defined as $\dot{\sigma} = \sum_{i=1}^{N_s}(\sigma_i * DY_i/Dt)$ (Shepherd 2009), where, $\mathrm{N_s}$ is the number of species, $\mathrm{Y_i}$ is the mass fraction of species, where **i** and σ_i is the thermicity coefficient of species **i** defined for ideal gas as $\sigma_i = \overline{W}/W_i - h_i\,(T)/C_P\,(T)\,T$ (Shepherd 2009). In addition, $\mathrm{W_i}$ is the molecular weight of species i, T is the static temperature, $\mathrm{C_P}$ is the mixture specific heat at constant pressure and $\mathrm{h_i}$ is the species standard state enthalpy. The thermicity length scale can be defined as shown in Figure 1 and is equivalent to the reaction zone thickness in deflagration flames. For comparisons, the $\dot{\sigma}$ definition is used consistently for both detonation and deflagration to define the induction and thermicity scales.

The temperature and thermicity profiles for the detonation and the deflagration waves are compared in Figure 1(b). We define the flame width to be the distance between the unburnt mixture just before any heat addition (i.e., shock location for detonation) to the location where the products' temperature vary only within 1% (i.e., flame temperature). Results show that the overall detonation structure width is about one-tenth of the deflagration flame. The flame temperature is also 27% higher in detonation due to the initial shock thermal effect compared to deflagration. Results show that compared to deflagration, detonation has a propagation speed that is three orders of magnitude larger (i.e., 2.33 m/s versus 1968.12 m/s), has an induction length scale that is one order of magnitude shorter (i.e., 3.6 mm versus 0.14 mm), an induction time scale that is five orders of magnitude faster (i.e., 400 μs versus 0.375 μs) and a thermicity width that is one order of magnitude smaller (i.e. 0.29 mm versus 0.047 mm). In addition to the induction timescale, we can define a chemical timescale that is an inverse of thermicity. Deflagration exhibits two orders of magnitude slower chemical timescale compared to deflagration (i.e., 77 μs versus 0.213 μs). As such, detonation exhibits faster rates of chemical kinetics and potential higher thermal efficiency due to the wave pressurization and temperature preheating effect. Faster rates of chemical kinetics for detonation are key for regime identification criterion.

3. Chemical explosive mode analysis for regime identification

CEMA provides a method for studying the ignition modes and the contribution of species and reactions to ignition (Lu *et al.* 2010). Given a state vector $\Phi = [\mathrm{T}, \mathrm{Y_i}, ...\mathrm{Y_{Ns}}]$, the scalars transport in time t can be defined as the sum of the rate of transport due to diffusion and due to chemical reactions in the absence of other sources

$$\rho\frac{D\Phi}{Dt} = \dot{\Omega}_{\mathrm{diff}} + \dot{\Omega}_{\mathrm{reac}}\,, \tag{3.1}$$

where $D/Dt = \partial/\partial t \; + \; u_i\partial/\partial x_i$ is the material derivative and $\dot{\Omega}_{\mathrm{diff}}$ and $\dot{\Omega}_{\mathrm{reac}}$ are the state-vector change due to diffusion and chemical reactions, respectively.

The first step in CEMA is to compute the chemical Jacobian matrix (JAC) $\mathbf{J} = (\partial\Omega_{\mathrm{reac}}/\partial\Phi)$. The JAC eigenmodes can be identified by the eigenvalues λ in dimensions of 1/s, and

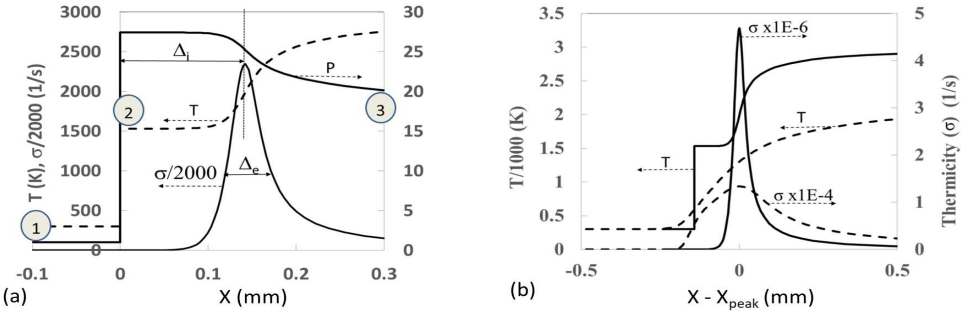

FIGURE 1. (a) The ZND detonation wave structure for H_2/air for $\phi = 1.0$, P = 1 bar, and T = 300 K. The numbers in circles refer to (1) the inflow condition, (2) the von Neumann [VN] state and (3) the sonic equilibrium CJ state where Δ_i is the induction length and Δ_e is the exothermic thermicity pulse width. (b) Temperature and thermicity profiles for the detonation ——— and deflagration – – –– waves. The origin for both is shifted to X_{peak} that represents the location of peak thermicity.

the left and right eigenvectors, i.e., V_l, and V_r, respectively. To characterize the chemical explosive modes, the eigenvalues are sorted in descending order, and the chemical explosive modes' (CEM) eigenvalues λ_{cem} are defined as the eigenvalues with a positive real part (Lu *et al.* 2010), $[Re(\lambda) > 0]$. The fastest growing chemical mode is then defined as the maximum CEM local eigenvalue, $[\lambda_{\text{exp}} = max(Re(\lambda_{\text{cem}}))]$. If the maximum real part is negative, then the mixture is in the post-ignition mode.

As such, the chemical Jacobian matrix eigenvalues λ can be used to detect the mixture state of ignition. A positive explosive eigenvalue (i.e., λ_{cem}) indicates an explosive mixture mode that is tending to ignite, and a negative eigenvalue indicates a fully burned mixture mode that emerged from an ignited mixture. In an adiabatic ideal system, the zero-crossing ($\lambda_{\text{exp}} = 0$) will correspond to the ignition point.

Furthermore, CEMA can be used to identify the different contributions of chemical species to the chemical explosive modes through the normalized explosive index (**EI**) defined as $\mathbf{EI} = (\mathbf{diag}|\mathbf{V_{r,exp}V_{l,exp}}|)/\sum(\mathbf{diag}|\mathbf{V_{r,exp}V_{l,exp}}|)$ (Lu *et al.* 2010), where, $V_{r,exp}$ and $V_{l,exp}$ are the right and left eigenvector columns associated with λ_{exp} mode, respectively. At each grid point, for a coupled system of temperature and N_s species, **EI** will have $N_s + 1$ dimensions and is normalized between 0 and 1. A higher **EI** indicates a higher contribution to the CEM mode. Similarly, the contribution of reactions to the chemical explosive mode can be quantified by the participation index (**PI**) $\mathbf{PI} = |(\mathbf{V_l} \cdot \mathbf{M_{stoic}}) \otimes \mathbf{R}|/\sum(\mathbf{V_l} \cdot \mathbf{M_{stoic}}) \otimes \mathbf{R}$, where $\mathbf{M_{stoic}}$ is the stoichiometric coefficient matrix, **R** is the net rates of each reaction and $\otimes$ indicates element-wise multiplication (Xu *et al.* 2019). At each grid point, the **PI** vectors will have the dimension of N_r, where N_r is the number of reactions for a given chemical mechanism. Similar to **EI**, the **PI** elements at each grid point are normalized between 0 and 1. A higher **PI** indicates a higher reaction contribution to the chemical explosive mode.

CEMA is applied to the one-dimensional ZND detonation and a freely propagating premixed flame with equivalence ratio ϕ, P, and T fixed to 1.0, 1.0 bar and 300 K, respectively. The explosive eigenvalue profiles across the detonation and deflagration are shown in Figure 2. The explosive eigenvalues are superimposed with the temperature profiles in Figure 2(a,b) and with several key species profiles in Figure 2(c,d). The results show that the explosive eigenvalue is positive before ignition, crosses zero near the

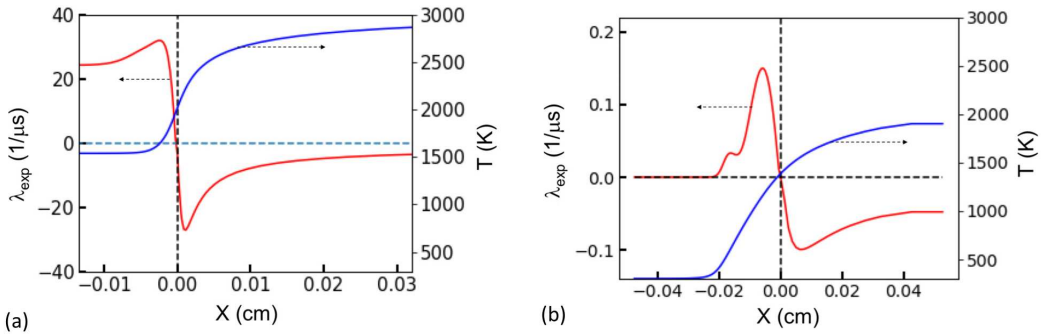

FIGURE 2. Wave structures visualized by the static temperature and CEM eigenvalue λ_{exp} profiles for (a) detonation and (b) deflagration. The graphs are centered at the $\lambda_{\text{exp}} = 0$ point.

peak value of H and OH radicals and becomes negative in post-ignition. The explosive eigenvalue is two orders of magnitude higher in detonation compared to deflagration. Both detonation and deflagration show an induction zone where the temperature and the explosive eigenvalue are approximately constant. In the induction zone, the explosive eigenvalue is zero in deflagration and is equal to the peak value in detonation, where the chain branching reactions are initiated immediately after the shock. This phenomenon is referred to as radical explosion (Lu *et al.* 2010). As temperature increases in the induction region, the explosive eigenvalue increases to a peak maximum value and then decreases toward the ignition point (i.e., zero crossing). The region between the peak value and ignition point represents a zone where the net chemical production rate is decreasing and thermal and mass diffusion become more important. After the ignition point, the eigenvalue decreases to a minimum and then increases but remains negative in the burned mixture.

To identify the contribution of different species and chemical reactions to the chemical explosive mode, the explosive index (**EI**) and the participation index (**PI**) across detonation and deflagration are shown in Figure 3. In the deflagration, the temperature contribution to the explosive mode dominates the reactants zone. As the ignition point is approached, the H radical contribution becomes nearly equal to temperature then decreases due to diffusion from the reaction zone (Lu *et al.* 2010). In detonation, however, we observe a trend behind the shock that is similar to auto-ignition in zero-dimensional constant-pressure reactors, where the H contribution dominates across the induction zone. This behavior indicates radical explosion rather than thermal explosion, as observed in deflagration waves (Lu *et al.* 2010). Examining the **PI** profiles, we observe that the reaction $H + O_2 <=> O + OH$ has the dominant contribution in detonation due to the abundance of H and O_2. In deflagration, however, in the preheat zone the two reactions $H_2 + OH <=> H + H_2O$ and $HO_2 + OH <=> H_2O + O_2$ have the highest contribution to the explosive mode. Following the preheat zone, as H radicals accumulate, the reaction $H + O_2 <=> O + OH$ dominates the explosive mode, similar to detonation. As observed, the H radical shows the highest explosive index among the other radicals in both deflagration and detonation and therefore can be used as an ignition indicator for both modes. In the following Damköhler number analysis, the H radical is used as an ignition indicator to represent the reaction and induction zones.

Figure 4 shows the variation over a wide range of equivalence ratios for the maximum and minimum of the CEM eigenvalues for both deflagration and detonation. Deflagration

consistently shows lower maximum (positive) CEM eigenvalues and higher minimum (negative) CEM eigenvalues for different equivalence ratios. The plot shows that CEMA can be used successfully to detect detonation and deflagration. However, one challenge for CEMA as a regime identifier is the need to compute deflagration a-priori to the simulation at constant pressures. This might be challenging in real propulsion devices, which may have a wide range of local pressure conditions different than the inflow values. For a example, as shown in Figure 1 for an inflow pressure of 1 bar, the local pressure can range from 27 bar after the shock to 15 bar at the sonic plane. In this case, a range of CEMA deflagration solutions at different pressures will be needed for local detection. The criterion introduced in the next section computes a local threshold that is common across different pressures to detect deflagration.

4. Characteristic Damköhler number as a regime identifer

To distinguish deflagration and detonation, a characteristic Damköhler number based on the H radical is defined as

$$Da_{c,H} = \frac{\dot{\Omega}_{\mathrm{H,reac,max}}}{\dot{\Omega}_{\mathrm{H,diff,max}}}, \tag{4.1}$$

where $\Omega_{\mathrm{H,reac,max}}$ and $\Omega_{\mathrm{H,diff,max}}$ are the peak chemical and diffusion rates, respectively as defined in Eq. (3.1).

The criterion is examined at different mixture pressures and equivalence ratios. The deflagration and detonation rates of diffusion and chemical kinetics rates are compared for P = 1 bar and P = 10 bar. The net chemical reaction rates and diffusion source terms for the H radical are compared for P = 1 bar in Figure 5 and P = 10 bar in Figure 6. For P = 1 bar, compared to deflagration, detonation shows significantly larger chemical kinetic rates (by four orders of magnitude), larger diffusion rates (by two orders of magnitude), higher thermicity (by two orders of magnitude) and higher heat release rate (by three orders of magnitude). Deflagration also shows that each of these values is more broadly diffused in space compared to detonation. Similarity, the 10-bar plots show that the chemical reaction rates for detonation are four orders of magnitude larger than deflagration. The diffusion source term, however, is only one order of magnitude higher for detonation at P = 10 bar. Therefore, the rate of increase of diffusion with respect to pressure is higher in deflagration than detonation for the H radical. That is expected due to the different nature of ignition and propagation mechanisms between detonation and deflagration, as discussed earlier. In detonation waves, diffusion is known to have a secondary effect compared to both kinetics and the coupling mechanism between the shock and the flame (Zel'dovich 1980). In deflagration waves, however, heat and mass diffusion balanced with heat produced by chemical reaction is important to sustain flame propagation. In deflagration, the rate of the thermal and mass diffusion increases with pressure, while in detonation the initial radical explosion shown earlier leads to an abundance of radicals, third body collisions and almost constant temperature after the shock, as well as lower mass and thermal diffusion compared to deflagration.

The variation of the characteristic Damköhler number with ϕ and P is compared in Figure 7. For deflagrations, the H radical characteristic Damköhler number is in O(1) at different equivalence ratios and pressures. For detonations, the characteristic Damköhler number is O(100) for P = 1 bar and O(1000) for P = 10 bar. As discussed, this disparity in $Da_{\mathrm{c,H}}$ is due to the difference in ignition mechanisms in which detonation undergoes

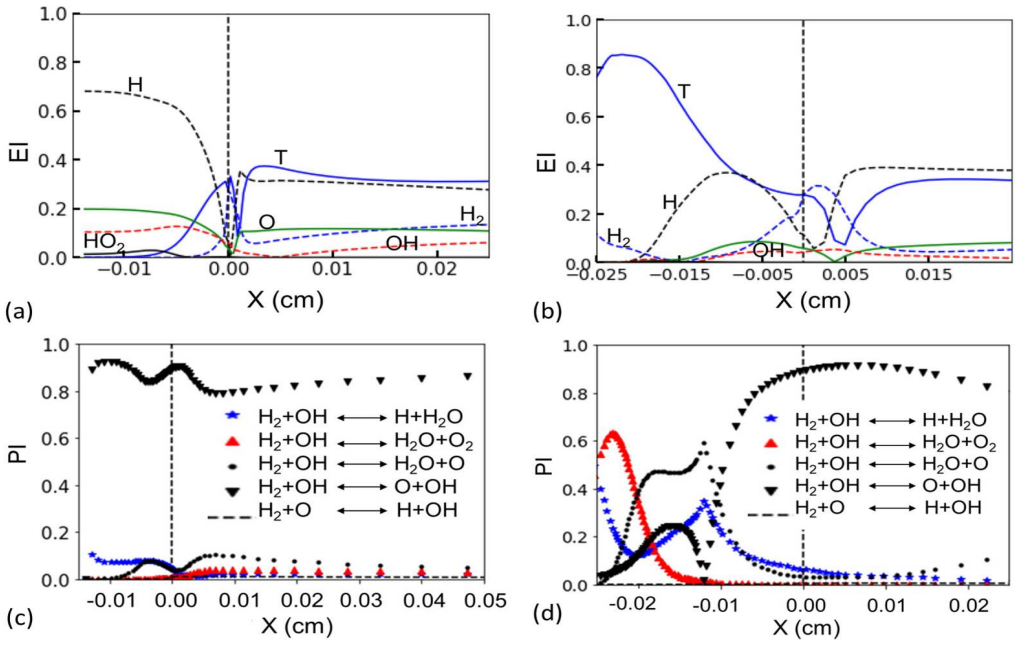

FIGURE 3. Explosive index (**EI**) for (a) detonation and (b) deflagration and participation index (**PI**) for (c) detonation and (d) deflagration.

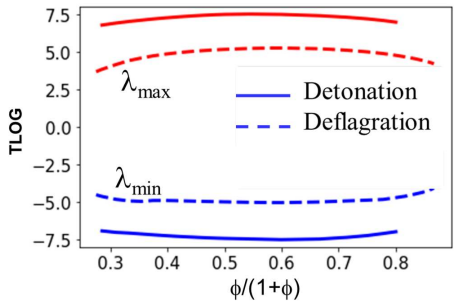

FIGURE 4. Comparing detonation and deflagration maximum and minimum CEM at P = 1 bar, where TLOG = $sign\,(\lambda_{\rm exp})\mathrm{x}log10\,(1+|\lambda_{\rm exp}|, 1/\mathrm{s})$.

radical explosion after the shock and deflagration undergoes thermal explosion followed by radical explosion (Lu *et al.* 2010). Therefore, the characteristic Damköhler number based on the H radical can be used as a detection criterion for detonation and deflagration, where a Damköhler number on the order of unity (<3) indicates deflagration-based combustion and higher values (>100) will indicate detonation-based combustion.

Finally, the method is applied to the non-premixed AFRL 6-inch RDE setup (Rankin *et al.* 2017). The hybrid RANS-LES simulation for the test rig is reported earlier (Elasrag *et al.* 2022). Figure 8 shows unwrapped contour plots for the outer wall. The x-axis is the circumferential angle along the unwrapped circular cross section and the y-axis is the height of the detonation channel in millimeters, where the detonation is propagating from left to right. Figure 8(a-e) shows contours of P, T, ϕ and heat release rate, as well as the Damköhler number limited by 2 and by 100, respectively.

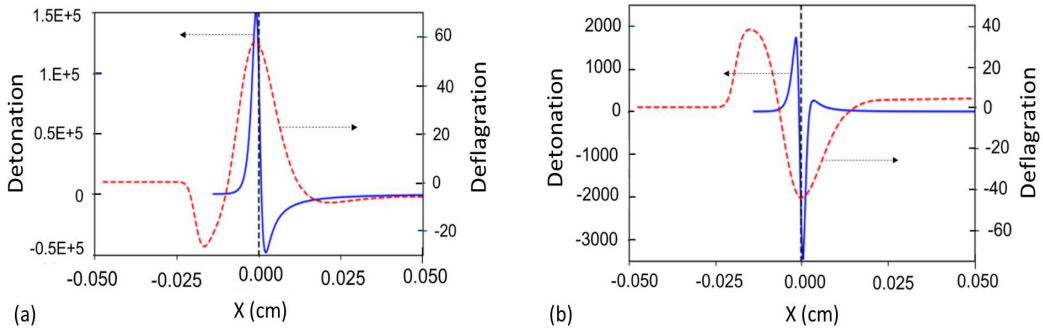

FIGURE 5. Comparing detonation and deflagration H radical (a) net chemical production rates $\Omega_{\text{reac,H}}$ and (b) diffusion source terms $\Omega_{\text{diff,H}}$ in kmole/m^3/s for P = 1 bar.

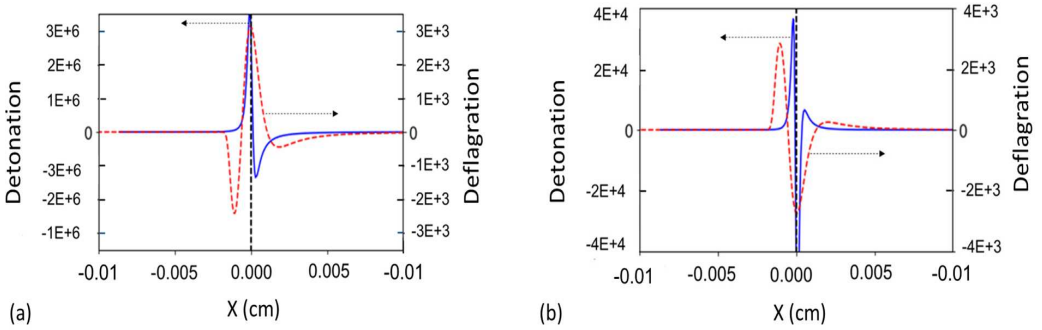

FIGURE 6. Comparing detonation and deflagration H radical (a) net chemical production rates $\Omega_{\text{reac,H}}$ and (b) diffusion source terms $\Omega_{\text{diff,H}}$ in kmole/m^3/s for P = 10 bar.

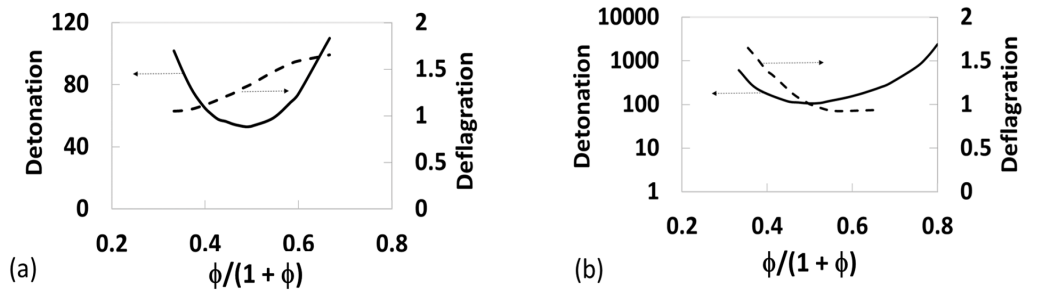

FIGURE 7. Comparing the detonation and deflagration critical Damköhler number for (a) P = 1 bar, and (b) P = 10 bar at different equivalence ratios ϕ.

As illustrated in Figure 8(a,b), the RDE flow field shows different zones: zone-D, where the detonation front is located, zone-P behind the detonation wave that contains the high-temperature products from the current detonation cycle, zone-F for the fresh reactants mixture, and zone-G for the products left from the previous detonation cycle. A cycle is defined here as a complete rotation of the detonation wave around the channel.

The heat release rate spectrum shows that heat is released at low pressure ahead of the detonation wave at the edge of the fresh mixture (zone-F) and the previous cycle

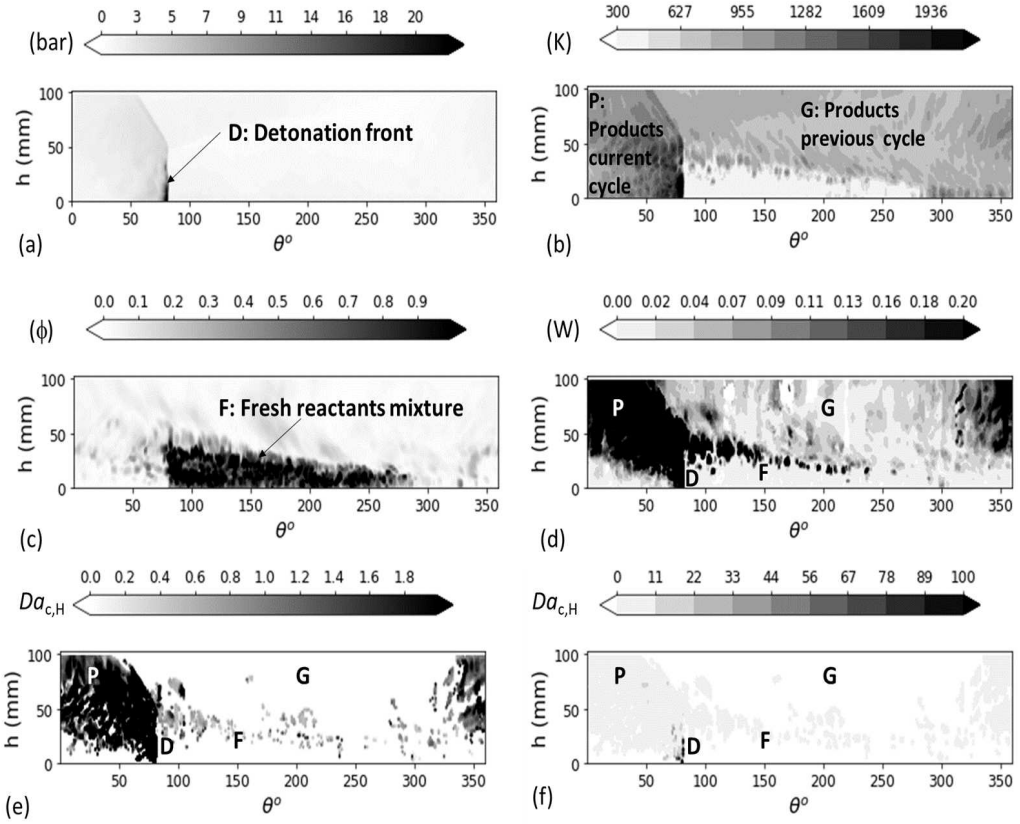

FIGURE 8. Contours for the unwrapped channel outer wall of the AFRL 6-inch RDE from Elasrag *et al.* (2022) and Rankin *et al.* (2017) for (a) static pressure P (bar), (b) static temperature T (K), (c) equivalence ratio ϕ, (d) heat release rate $\dot{Q}$(W) , (e) $Da_{c,H}$ limited by 2 and (f) $Da_{c,H}$ limited by 100.

products (zone-D). Similar to one-dimensional analysis, Figure 8(e,f) shows that in the low-pressure region, the Damköhler number is on the order of unity and is on the order of 100 at the detonation front (zone-D). As such, the Damköhler criterion can successfully detect the detonation and deflagration burning.

5. Conclusions

Using the dominant radical (i.e., H) to the chemical explosive mode, a characteristic Damköhler number is defined to successfully distinguish deflagration in a detonative mixture. Detonation ignition shows an opposite trend to deflagration ignition, where a radical explosion is initiated by the shock followed by thermal runaway. In RDEs, deflagration is found to be initiated between the refill fresh mixture and the burned mixture from the previous detonation cycle.

Acknowledgments

The work is supported by the Air Force Research Laboratory and is approved for public release; distribution is unlimited.

REFERENCES

Chacon, F. & Gamba, M. 2019 Study of parasitic combustion in an optically accessible continuous wave rotating detonation engine. *AIAA Paper* 0473.

Cocks, P., Holley, A. & Rankin, B. 2016 High fidelity simulations of a non premixed rotating detonation engine. *AIAA Paper* 0125.

Conaire, M., Curran, H., Simmie, J., Pitz, W. & Westbrook, C. 2004 A comprehensive modeling study of hydrogen oxidation. *Int. J. Chem. Kinet.* **36**, 603–622.

Elasrag, H. A., Gallagher, T., Rankin, B. & Schumaker, A. S. 2022 Stress blended eddy simulations for hydrogen-air rotating detonation engine with wall heat transfer. *ASME-GT Paper* 81152.

Elasrag, H. A. & Ju, Y. 2013 Direct numerical simulations of NOx effect on multistage autoignition of DME/air mixture in the negative temperature coefficient regime for stratified HCCI engine conditions. *Combust. Flame* **161**, 256–269.

Kaneshige, M. J. & Shepherd, J. E. 1996 Oblique detonation stabilized on a hypervelocity projectile. *Proc. Combust. Inst.* **26**, 3015–3022.

Lu, F. K. & Braun, E. M. 2014 Rotating detonation wave propulsion: experimental challenges, modeling, and engine concepts. *J. Prop. Power* **30**, 1125–1142.

Lu, T. F., Yoo, C. S., Chen, J. H. & Law, C. K. 2010 Three-dimensional direct numerical simulation of a turbulent lifted hydrogen jet flame in heated coflow: a chemical explosive mode analysis. *J. Fluid Mech.* **652**, 45–64.

Luo, Z., Yoo, C. S., Richardson, E. S., Chen, J. H., Law, C. K. & Lu, T. 2012 Chemical explosive mode analysis for a turbulent lifted ethylene jet flame in highly-heated coflow. *Combust. Flame* **159**, 265–274.

Pal, P., Valorani, M., Arias, P. G., Im, H. G., Wooldridge, M. S., Ciottoli, P. P. & Galassi, R. M. 2020 Computational characterization of ignition regimes in a syngas/air mixture with temperature fluctuations. *Proc. Combust. Inst.* **36**, 3705–3716.

Rankin, B. A., Richardson, D. R., Caswell, A. W., Naples, A. G., Hoke, J. L. & Schauer, F. R. 2017 Chemiluminescence imaging of an optically accessible nonpremixed rotating detonation engine. *Combust. Flame* **176**, 12–22.

Shepherd, J. E. 2009 Detonation in gases. *Proc. Combust. Inst.* **32**, 83–89.

Strakey, P., Ferguson, D., Sisler, A. & Nix, A. 2016 Computationally quantifying loss mechanisms in a rotating detonation engine. *AIAA Paper* 0900.

Wolanski, P. 2013 Detonative propulsion. *Proc. Combust. Inst.* **34**, 125–158.

Xu, C., Park, J., Yoo, C., Chen, J. H. & Lu, T. 2019 Identification of premixed flame propagation modes using chemical explosive mode analysis. *Proc. Combust. Inst.* **37**, 2407–2415.

Yoo, C. S., Luo, Z., Lu, T., Kim, H. & Chen, J. H. 2013 A DNS study of ignition characteristics of a lean iso-octane/air mixture under HCCI and SACI conditions. *Proc. Combust. Inst.* **34**, 2985–2993.

Zel'dovich, Y. B. 1940 On the theory of the propagation of detonations on gaseous system. *J. Exp. Theor. Phys.* **10**, 542–568.

Zel'dovich, Y. B. 1980 Regime classification of an exothermic reaction with nonuniform initial conditions. *Combust. Flame* **39**, 211–214.